



This is a repository copy of *Performance investigation of consequent-pole PM machines with E-core and C-core modular stators*.

White Rose Research Online URL for this paper:  
<https://eprints.whiterose.ac.uk/165309/>

Version: Accepted Version

---

**Article:**

Zhou, R., Li, G.-J. [orcid.org/0000-0002-5956-4033](https://orcid.org/0000-0002-5956-4033), Zhang, K. et al. (3 more authors) (2021) Performance investigation of consequent-pole PM machines with E-core and C-core modular stators. *IEEE Transactions on Energy Conversion*, 36 (2). pp. 1169-1179. ISSN 0885-8969

<https://doi.org/10.1109/TEC.2020.3027366>

---

© 2020 IEEE. Personal use of this material is permitted. Permission from IEEE must be obtained for all other users, including reprinting/ republishing this material for advertising or promotional purposes, creating new collective works for resale or redistribution to servers or lists, or reuse of any copyrighted components of this work in other works. Reproduced in accordance with the publisher's self-archiving policy.

**Reuse**

Items deposited in White Rose Research Online are protected by copyright, with all rights reserved unless indicated otherwise. They may be downloaded and/or printed for private study, or other acts as permitted by national copyright laws. The publisher or other rights holders may allow further reproduction and re-use of the full text version. This is indicated by the licence information on the White Rose Research Online record for the item.

**Takedown**

If you consider content in White Rose Research Online to be in breach of UK law, please notify us by emailing [eprints@whiterose.ac.uk](mailto:eprints@whiterose.ac.uk) including the URL of the record and the reason for the withdrawal request.



[eprints@whiterose.ac.uk](mailto:eprints@whiterose.ac.uk)  
<https://eprints.whiterose.ac.uk/>

# Performance Investigation of Consequent-Pole PM Machines with E-core and C-core Modular Stators

R. Zhou, G. J. Li, *Senior Member, IEEE*, K. Zhang, Z. Q. Zhu, *Fellow, IEEE*, M. P. Foster, and D. A. Stone  
 Department of Electronic and Electrical Engineering, The University of Sheffield, Sheffield, UK  
[g.li@sheffield.ac.uk](mailto:g.li@sheffield.ac.uk)

**Abstract**— This paper investigates some novel modular consequent pole PM machines (CPMs) with E-core and C-core stators. Different slot-pole number combinations including 12-slot/10-pole ( $N_s > 2p$ ) and 12-slot/14-pole ( $N_s < 2p$ ) have been investigated. Their static and dynamic electromagnetic performances have been investigated, e.g. the phase back-EMF, on-load torque, torque-speed curves, power factor-speed curves and also efficiency maps are compared. It is found that the existence of flux gaps (FGs) can improve the average torque of the 12-slot/14-pole E-core modular CPMs while the C-core structure can be a better candidate where relatively low torque ripple is desirable. Moreover, by selecting proper FG width, the 12-slot/14-pole E-core modular CPMs can achieve better flux-weakening capability and higher efficiency while the 12-slot/10-pole C-core modular CPMs can have higher power factors over the whole speed range. The finite element simulation results have been validated by a series of experiments using 12-slot/14-pole modular CPMs with both C-core and E-core stators.

**Index Terms**— Consequent-pole, C-core, E-core, modular, permanent magnet machines.

## I. INTRODUCTION

PERMNET magnet (PM) machines have been widely used in various applications such as electric vehicles and hybrid electric vehicles (EVs and HEVs), more electric aircraft and renewables, etc. thanks to their advantages in terms of high torque/power density and high efficiency [1]. However, due to the increasing cost and potential supply shortage of rare-earth PM materials such as NdFeB, machines with less or no PM materials have been an important research topic in recent years. In [2], it is suggested that the consequent pole (CP) concept might be a reasonable cost-saving solution. It is found that by adopting the CP rotor, approximately 33% of PM materials can be saved while achieving almost the same performance compared to the conventional surface mounted permanent magnet (SPM) machines. A novel CP flux-reversal PM (FRPM) machine is proposed in [3] for EV applications. It is founded that the proposed machine can produce a rated torque 26% higher than that of the conventional FRPM machine whilst its magnet consumption is halved. In [4], by using a CP inner stator in a partitioned-stator (PS) FRPM machine, the machine can achieve nearly 95% torque density of that with SPM inner stator while ~30% PM materials can be saved. A CP rotor is adopted in [5] to enhance the torque capability of the proposed hybrid dual-PM machine used for EVs.

Although the CPMs have aforementioned advantages, some intrinsic issues of the CP structure exist such as the even-order harmonics in the open-circuit air-gap flux density and phase back-EMFs, the unipolar shaft flux leakage, etc. To address these issues, several effective solutions have been proposed in

recent literature. In [6], it is demonstrated that the even-order harmonics in back-EMFs in the CPMs with specific slot/pole number combinations can be suppressed by using the multi-layer windings. It is also found in [7, 8] that the even-order harmonics in the back-EMFs and the unipolar shaft flux leakage can be mitigated by some hybrid rotors where the sequences of the magnet polarities are changed. Some other works have been done aiming to further improve the electromagnetic performances of the CPMs. In [9], a mechanical modular consequent-pole rotor is proposed to provide strong flux-focusing effect and the leakage flux near iron bridges can be significantly reduced. Results show that the torque density and the PM material utilization can be improved while similar torque ripple and efficiency can be achieved compared with the conventional counterparts. Moreover, in [10], a CPM with dovetailed CP rotor and quasi-trapezoidal PMs is proposed. By adopting this structure, the non-magnetic sleeve for magnet protection would not be required in high-speed applications. This can significantly reduce the total rotor losses compared with the conventional SPMs which often have significant sleeve losses. In addition, it is found that due to the removal of rotor sleeve and lower airgap reluctance, the proposed machine can have 3% higher average torque with nearly 20% less PM consumption compared with the conventional SPM.

Apart from the electromagnetic performances, the mechanical aspect and manufacturing process also need to be considered when designing electric machines, especially in wind power applications. This is because most wind power generators have large dimensions which makes the manufacturing process difficult. To cope with such challenges, a modular PM wind generator with E-core stator and segmented rotor is proposed in [11]. Another new single tooth segmented stator core without laminated-joint has been proposed in [12]. The laminated tooth modules with pre-wound coils are coupled with a solid back iron, which can significantly ease the winding process and also increase the slot fill factor. However, considerable iron losses in the solid stator holder makes such topologies less attractive in large machines. Moreover, other novel modular PM machines with so-called ‘flux gaps (FGs)’ inserted in alternate stator teeth have also been proposed in [13] and [14]. Such modular machines have been investigated thoroughly in [14-16]. It is concluded that the electromagnetic performances of the machines with slot number ( $N_s$ ) lower than pole number ( $2p$ ) can be improved by selecting an appropriate FG width. In such E-core modular machines, the average torque can be significantly increased without extra PM material consumption. Apart from the E-core modular structure, in [6], it is found that the C-core modular machine with surface-

mounted PM (SPM) rotor is a better candidate in applications where low torque ripple is desirable while the average torques could be slightly sacrificed.

The modular structures proposed in [14-16] provide a possibility to boost the average torque of conventional SPM machines. This means that to maintain the same torque level, the PM usage can be effectively reduced by utilizing the modular stator structure. Meanwhile, in previous sections it has been reported that the CP concept can be a cost-saving solution. Therefore, it is worth combining the modular stator with the CP rotor to achieve an even higher PM utilization and also potentially easier manufacture, assembly and transportation processes for large-dimension machines. This is the main novelty and contribution of this paper. Although the E-core modular CPMs have been compared with the modular inset SPM machines in [17], the investigation is far from being complete and only the static performances are investigated. Except for the E-core modular structure, the C-core modular CPMs will also be investigated in this paper. The operating principle of the investigated modular CPMs will be introduced based on mathematical modelling, and the phase back-EMF and electromagnetic torque production mechanisms will be analysed. Moreover, the dynamic performances such as on-load losses, torque-speed curves, power-speed curves and efficiency maps will be investigated for modular machines with different slot/pole number combinations. In addition, some design guidelines and recommendations will be given in the conclusion for machine designers to select the best modular CPMs for different applications with different requirements.

## II. DESIGN FEATURES AND OPERATION PRINCIPLE OF MODULAR CPMs

The topologies of E-core and C-core modular CPMs are shown in Fig. 1, where all machines have single layer concentrated winding structures. By way of example, only the 12-slot/10-pole and 12-slot/14-pole are chosen for investigations in this paper. Since the focus is on the influence of modular stator structures, some general design specifications are kept the same for all the investigated machines, as listed in Table 1. It is also worth noting that the total PM volume of each machine is the same for a fairer comparison. In addition, the PM thicknesses of the non-modular CPMs are optimized with the aim of achieving the highest torque at the rated current. Since the total PM volume is fixed, the PM pole arc to pole pitch ratio can be easily determined according to the optimal PM thickness. As a result, the optimal PM thicknesses of the machines with 12-slot/10-pole and 12-slot/14-pole are 2.7mm and 2.5mm, respectively.

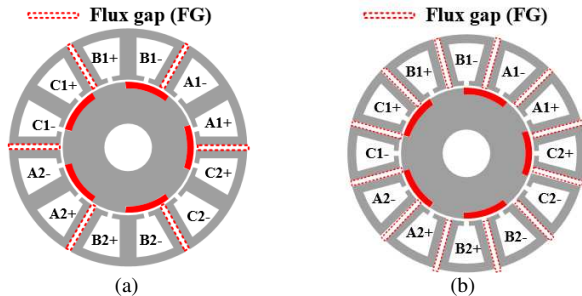


Fig. 1. Cross-sections of the investigated modular 12-slot/10-pole CPMs. (a) E-core stator, (b) C-core stator. The 14-pole machines have very similar structure.

Table 1 General specifications of the modular CPMs

Stator outer radius (mm)	50	Split ratio	0.57
Tooth body width (mm)	7.2	Stator yoke height (mm)	3.7
Air-gap length (mm)	1	Stack length (mm)	50
Rated current ( $A_{rms}$ )	7.34	Number of turns per phase	132

For the CPMs (modular or not), their operating principle can be explained using the following mathematical models. The PM excited MMF generated by the CP rotor shown in Fig. 1 can be expressed by [18]:

$$f_{PM}(\theta, t) = \sum_{i=1,2,3\dots}^{\infty} F_{PM_i} \cos[ip_r(\theta - \omega_r t)] \quad (1)$$

where  $F_{PM_i}$  is the  $i$ -order Fourier coefficients of PM generated MMF,  $p_r$  is the rotor pole pair number,  $\theta$  is the mechanical position in stationary coordinate,  $\omega_r$  is the rotor speed and  $t$  is the time. Moreover, the airgap permeance model considering both stator slot openings and also flux gaps can be expressed as:

$$\Lambda_s(\theta) = \sum_{j=0,1,2\dots}^{\infty} \Lambda_{s_j} \cos(jN_{s\_equiv}\theta) \quad (2)$$

where  $\Lambda_{s_j}$  is the  $j^{\text{th}}$ -order Fourier coefficients of the airgap permeance model considering both stator slot openings and also flux gaps,  $N_{s\_equiv}$  is the equivalent number of stator slots. It should be noted that introducing the FGs in modular machines could change the periodicity of airgap permeance and this is the reason why the equivalent number of stator slots  $N_{s\_equiv}$  is used to replace the actual number of stator slots in (2). In addition,  $N_{s\_equiv}$  are 12, 6 and 12 for non-modular, E-core and C-core modular machines, respectively.

With the PM excited MMF and airgap permeance, the air-gap flux density produced by the PMs can be derived as:

$$B_{ag\_PM}(\theta, t) = f_{PM}(\theta, t)\Lambda_s(\theta) \\ = \sum_{i=1,2,3\dots}^{\infty} \sum_{j=0,1,2\dots}^{\infty} B_{PM(i,j)} \cos[(ip_r \pm jN_s)\theta - ip_r\omega_r t] \quad (3)$$

Then, the phase back-EMF can be calculated by:

$$E_{ph}(t) = -\frac{d}{dt} [r_{ag} l_s \int_0^{2\pi} B_{ag\_PM}(\theta, t) N_{ph}(\theta) d\theta] \quad (4)$$

where  $r_{ag}$  is the air-gap radius,  $l_s$  is the stack length and  $N_{ph}$  is the phase winding function.  $N_{ph}$  for both the 12-slot/14-pole and 12-slot/10-pole single layer windings shown in Fig. 1 is the same and can be expressed as:

$$N_{ph}(\theta) = \sum_{m=1,3,5\dots}^{\infty} N_{ph_m} \cos(m\theta) \quad (5)$$

According to [18], only the harmonics such as the 1<sup>st</sup>, 5<sup>th</sup> (fundamental for 10-pole), 7<sup>th</sup> (fundamental for 14-pole), 11<sup>th</sup>... exist. Other triplen harmonics are cancelled in three-phase windings. With (3)-(5), the fundamental phase back-EMFs can be expressed in (6), which are not zero if  $m_{PM}$  satisfies (7).

$$E_{ph\_PM}(t) = r_{ag} l_s \sum_{i=1,2,3\dots}^{\infty} \sum_{j=0,1,2\dots}^{\infty} \sum_{m=|ip_r \pm jN_{s\_equiv}|} E_{PM(i,j)} \cos(ip_r \Omega_r t) \quad (6)$$

$$m_{PM} = |p_r \pm jN_{s\_equiv}|, j = 0,1,2 \dots \quad (7)$$

It is evident that not only the fundamental harmonics, i.e. 5<sup>th</sup> order ( $p_r = 5$  for the 12-slot/10-pole machine) and 7<sup>th</sup> order ( $p_r = 7$  for the 12-slot/14-pole machine), other harmonics in the winding function listed in Table 2 also contribute to fundamental back-EMF.

	Non-modular	E-core stator	C-core stator
12-slot/10-pole	$ 5 \pm 12j =5^{\text{th}}, 7^{\text{th}}, 19^{\text{th}} \dots$	$ 5 \pm 6j =1^{\text{th}}, 5^{\text{th}}, 7^{\text{th}} \dots$	$ 5 \pm 12j =5^{\text{th}}, 7^{\text{th}}, 19^{\text{th}} \dots$
12-slot/14-pole	$ 7 \pm 12j =5^{\text{th}}, 7^{\text{th}}, 17^{\text{th}} \dots$	$ 7 \pm 6j =1^{\text{th}}, 5^{\text{th}}, 7^{\text{th}} \dots$	$ 7 \pm 12j =5^{\text{th}}, 7^{\text{th}}, 17^{\text{th}} \dots$

$$T_{em} = \frac{e_a i_a + e_b i_b + e_c i_c}{\omega_r} \quad (8)$$

Finally, according to (8), the electromagnetic torque can be calculated. Here  $i_a$ ,  $i_b$  and  $i_c$  are 3-phase currents.

### III. OPEN-CIRCUIT PERFORMANCES

#### A. Phase Back-EMFs

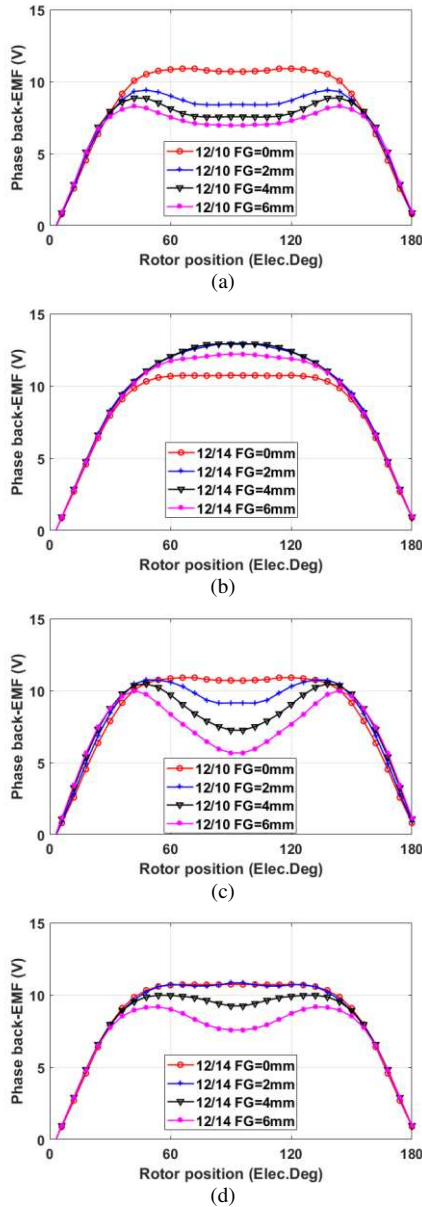


Fig. 2. Waveforms the phase back-EMFs of CPMs for different FG widths at 400 rpm. (a) 12-slot/10-pole E-core CPM, (b) 12-slot/14-pole E-core CPM, (c) 12-slot/10-pole C-core CPM, (d) 12-slot/14-pole C-core CPM.

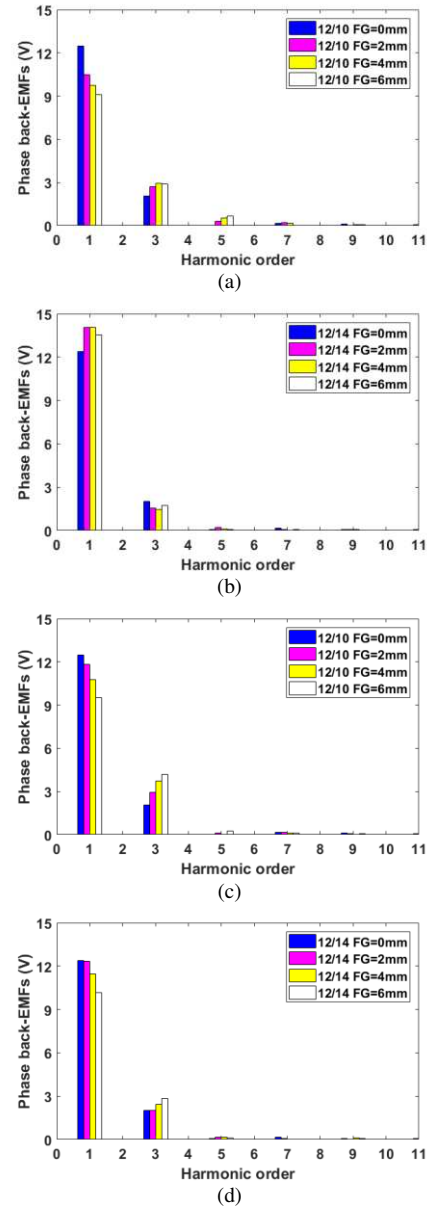


Fig. 3. Spectra of the phase back-EMFs of CPMs for different FG widths at 400 rpm. (a) 12-slot/10-pole E-core CPM, (b) 12-slot/14-pole E-core CPM, (c) 12-slot/10-pole C-core CPM, (d) 12-slot/14-pole C-core CPM.

The waveforms and spectra of the phase back-EMFs are shown in Fig. 3. It is found that for the 12-slot/10-pole modular

CPMs, the magnitude of fundamental phase back-EMF is decreasing with the increasing FG width, regardless of the E-

core or C-core structure. However, the C-core structure could weaken the influence of the FGs on the phase back-EMFs. As for the 12-slot/14-pole modular CPMs, the E-core and C-core structures have different influences. In terms of the E-core 12-slot/14-pole modular CPMs, the magnitude of fundamental phase back-EMF will first increase with the increasing FG width and then starts to decrease if the FG width continues to increase. This means that the FG has a ‘flux-focusing’ effect in the E-core 12-slot/14-pole modular CPMs with an appropriate FG width. However, the FG only has a negative effect on the C-core 12-slot/14-pole modular CPMs, i.e. the fundamental phase back-EMFs always decrease with the increasing FG width.

The different influences of FGs on the phase back-EMF will be reflected on the average torque as will be investigated in IV. Apart from the fundamental phase back-EMF, the 5<sup>th</sup> and 7<sup>th</sup> harmonics need to be analysed as they usually contribute to the torque ripple. In general, the higher the 5<sup>th</sup> and 7<sup>th</sup> back-EMF harmonics are, the higher the torque ripple would be. It is found that, the 5<sup>th</sup> and 7<sup>th</sup> order harmonics in the phase back-EMFs of the C-core modular CPMs are lower compared with those of the E-core modular CPMs, especially for the 12-slot/10-pole modular CPMs. Again, this influence is reflected on the torque ripple coefficient which will be investigated in the section IV.

B. Cogging Torque

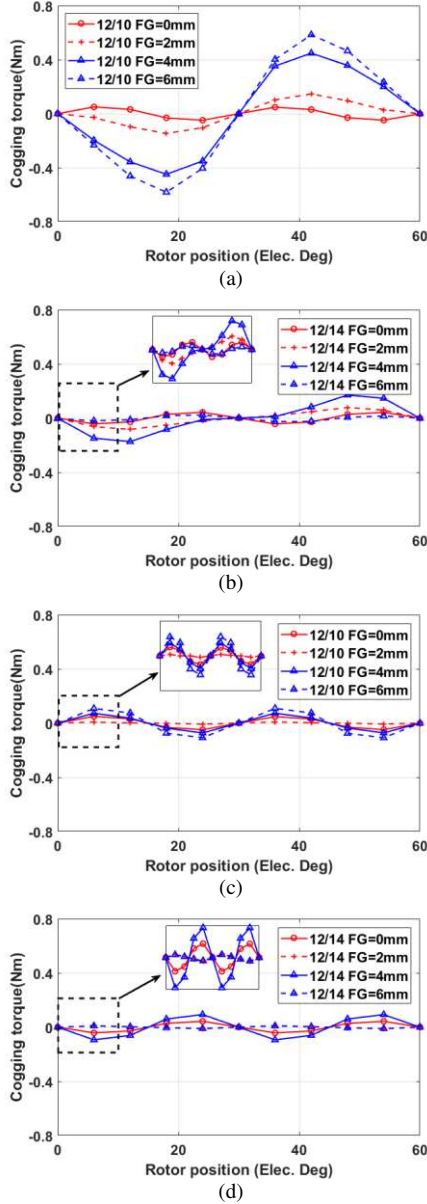


Fig. 4. Waveforms of the cogging torques. (a) 12-slot/10-pole E-core CPM, (b) 12-slot/14-pole E-core CPM, (c) 12-slot/10-pole C-core CPM, and (d) 12-slot/14-pole C-core CPM.

Apart from the phase back-EMF, it is also essential to evaluate the cogging torques. This is due to the fact that, compared to the 5<sup>th</sup> and 7<sup>th</sup> order harmonics in phase back-EMF,

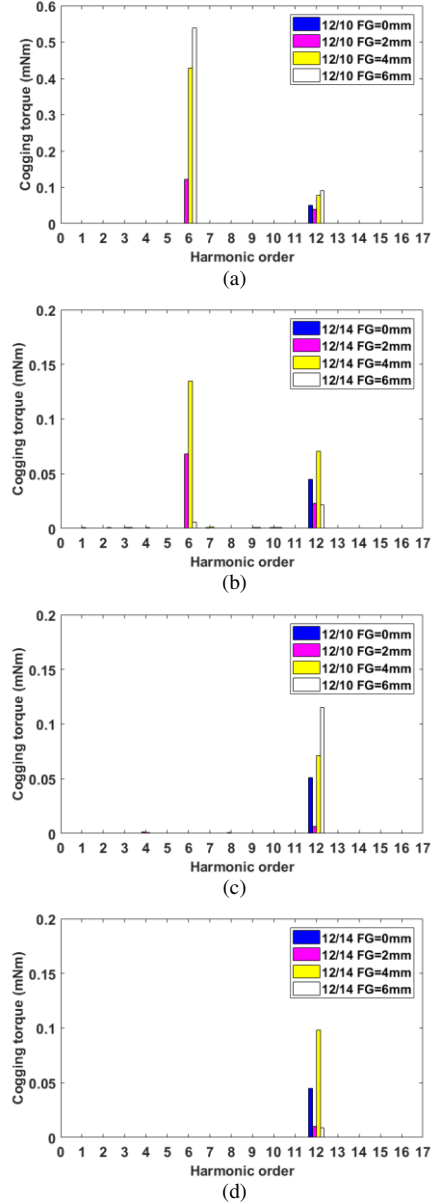


Fig. 5. Spectra of the cogging torques. (a) 12-slot/10-pole E-core CPM, (b) 12-slot/14-pole E-core CPM, (c) 12-slot/10-pole C-core CPM, and (d) 12-slot/14-pole C-core CPM.

the cogging torque might sometimes be a more dominant factor in the torque ripple. In order to figure out the influence of the FGs on the cogging torque, the waveforms and spectra of the

investigated E-core and C-core modular CPMs with different FG widths are shown in Fig. 4 and Fig. 5. It can be observed from the spectra that, the fundamental cogging torques for the E-core 12-slot/10-pole and 12-slot/14-pole CPMs change from 12<sup>th</sup> to 6<sup>th</sup> after introducing the FGs. However, the order of the fundamental cogging torques of the 12-slot/10-pole and 12-slot/14-pole C-core CPMs remain unchanged, which is the 12<sup>th</sup> order.

This can be explained by using the number of cogging torque cycles in one electrical period. It can be calculated by  $N_c = LCM(kp, N_s)/p$  [7], where  $LCM$  is the least common multiple (LMC),  $N_s$  is the number of stator slots,  $p$  is the number of rotor pole pairs, and for conventional CPMs in this paper,  $k = 1$ . As a result, the non-modular CPMs have 12 cycles in one electrical period. However, when the FGs are introduced, the slot number of E-core structure can be considered as 6 rather than 12 which can reduce the cycle number per electrical period from 12 to 6. For the C-core machines with 12 stator segments, the slot number can still be considered as 12 which means the cycle number will remain the same as 12.

Moreover, the peak-to-peak cogging torque versus the FG width of the investigated modular CPMs are shown in Fig. 6. It can be observed that the C-core CPMs have smaller peak-to-peak cogging torques compared with their E-core counterparts, regardless of the slot/pole number combination. This is mainly due to fact that, in general, the value of cogging torques are also determined by the LMC as discussed in [19]. It is generally valid that more cycles will lead to lower peak cogging torque. Therefore, by choosing a proper FG width (e.g. 2mm and 3mm) in the C-core CPMs, the cogging torque can be significantly reduced. It is worth noting that the different influences of FGs on cogging torque will be reflected on the torque ripple as will be investigated in the section IV.

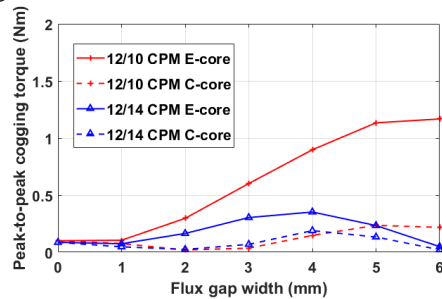


Fig. 6. Peak-to-peak cogging torque vs FG width of the investigated CPMs.

#### IV. ON-LOAD PERFORMANCES

##### A. On-Load Torques

The average torques and torque ripple coefficients of the investigated CPMs at rated condition against different FG widths are shown in Fig. 7. Similar to the phase back-EMF investigated previously, the FGs also have a significant torque improvement effect on the E-core 12-slot/14-pole CPM if a proper FG width is selected. Moreover, at small FG width (such as 1mm, 2mm), a very slight increase in the torque of the C-core 12-slot/14-pole CPM can be observed. However, for all the other machines with 12-slot/10-pole, the torque performance will be deteriorated with increasing FG width. In terms of the torque ripple, for all the modular CPMs, the adoption of C-core structure can reduce the torque ripple, especially for the 12-

slot/10-pole CPMs. This is due to the same reason as explained for the cogging torque in section III.B.

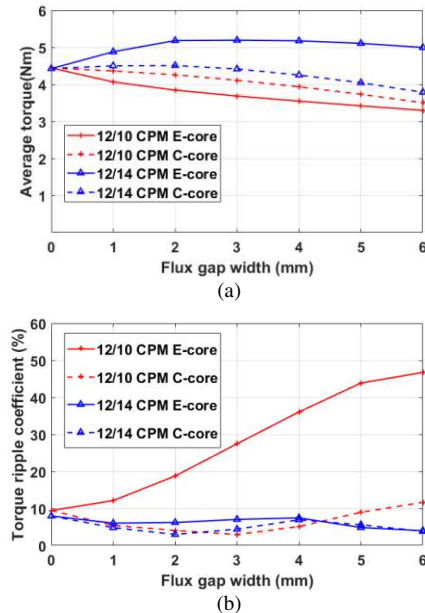


Fig. 7. (a) Average torque vs FG width, (b) torque ripple coefficient vs FG width of the investigated modular CPMs at the rated current ( $I_{rms}=7.34A$ ).

In order to figure out the overload capability and the saturation effect, the 12-slot/14-pole E-core CPM with 2mm FG width is chosen as an example. Its average torque versus phase RMS current has been calculated, as shown in Fig. 8. It can be seen that the torque will always increase with phase RMS current, but the slope of increase becomes smaller when  $I_{rms} > 15A$  phase RMS current, which is almost 2 times of the rated current.

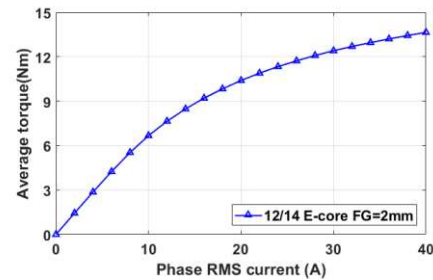


Fig. 8. Average torque vs phase RMS current of the 12-slot/14-pole E-core CPM (FG=2mm).

##### B. $d$ - and $q$ -Axis Inductances

The  $d$ - and  $q$ -axis inductances ( $L_d$  and  $L_q$ ) are generally important for analysing the dynamic performance and also flux weakening capability of PM machines. In order to account for the cross-coupling effect between the  $d$ - and  $q$ -axes for more accurate performance predictions, it is essential to evaluate  $L_d$  and  $L_q$  under different  $d$ - and  $q$ -axis currents ( $I_d$  and  $I_q$ ), i.e. different load conditions. Therefore,  $L_d$  and  $L_q$  versus  $I_d$  and  $I_q$  of the modular E-core and C-core CPMs with different FG widths have been calculated.

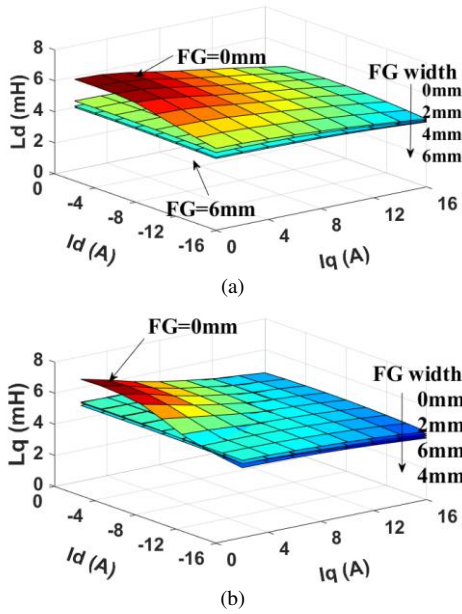


Fig. 9.  $L_d$  and  $L_q$  vs  $I_d$  and  $I_q$  for the modular E-core CPMs with 12-slot/14-pole. (a)  $L_d$ , (b)  $L_q$ .

C. Iron Losses and Magnet Eddy Current Loss

The FGs can be regarded as “dummy slots” on the stator iron core and may cause extra variation in the airgap permeance. This will have impact on the loss performances including stator and rotor core iron losses and PM eddy current losses. Since the E-core stator has 6 FGs whilst the C-core stator has 12 FGs, it is necessary to figure out the influences of different structures on the losses. Therefore, the stator iron losses and PM eddy current losses at rated condition are calculated and shown in Fig. 10.

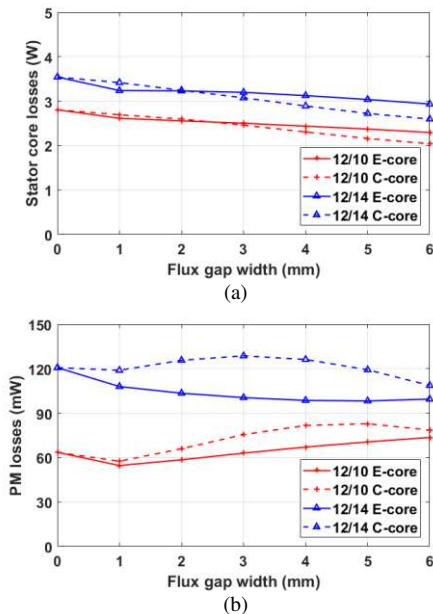


Fig. 10. (a) Stator iron losses vs FG width, and (b) PM eddy current losses vs FG width. The phase current is 7.34Arms and the rotor speed is 400rpm.

It can be observed that for all the investigated modular CPMs, the stator iron losses can be reduced by increasing the FG width and the C-core structure can reduce more stator iron losses than the E-core structure with larger FG width ( $\geq 2.5$ mm), regardless

of the slot/pole number combinations. This phenomenon can be explained by analyzing the spectra of on-load air-gap flux densities, as shown in Fig. 11.

It is apparent that the main working harmonics, e.g. the 5<sup>th</sup> order harmonic for the 12-slot/10-pole machines and the 7<sup>th</sup> order harmonic for the 12-slot/14-pole machines, are reducing with increasing FG width. Since the working harmonics are dominant in the stator iron losses, the stator iron losses will be reduced with increasing FG width.

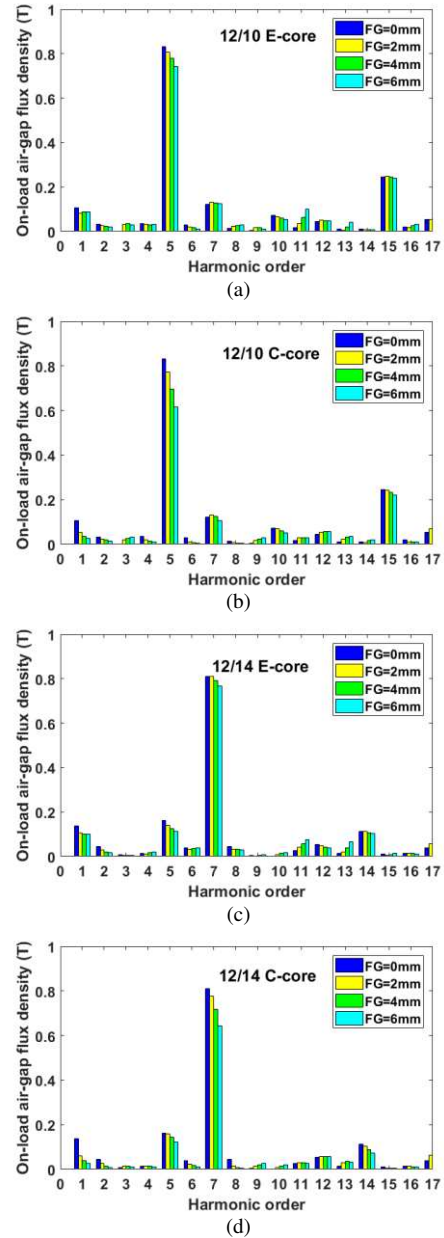


Fig. 11. Spectra of the on-load air-gap flux density of the 12-slot/10-pole modular CPMs and 12-slot/14-pole modular CPMs. (a) and (c) E-core, (b) and (d) C-core.

The PM eddy current losses are mainly caused by the sub-harmonics rather than the working harmonics. For the 12-slot/10-pole machines, although the 1<sup>st</sup> order harmonics are reduced slightly with the increasing FG width, some increase can be observed in the magnitudes of other dominant harmonics such as the 7<sup>th</sup>, 11<sup>th</sup> and 13<sup>th</sup>. Taking all these into account, for the 12-slot/10-pole CPMs, the FGs have nearly no positive

effect on the PM eddy current losses although they can be reduced very slightly at a 1mm FG width.

In terms of the 12-slot/14-pole E-core CPMs, most lower and dominant order harmonics such as 1<sup>st</sup>, 2<sup>nd</sup>, 5<sup>th</sup> and 8<sup>th</sup> order harmonics keep reducing with the FG width, this is the reason that the PM eddy current losses of the 12-slot/14-pole E-core CPMs are reduced with increasing FG width. However, for the 12-slot/14-pole C-core CPMs, the reduction in the magnitude of the 5<sup>th</sup> order harmonic is not significant when the FG width is smaller than 3mm, with a small increase in the 9<sup>th</sup> order harmonics at small FG width, the PM eddy current losses of the 12-slot/14-pole C-core CPMs will first increase slightly and then starts to decrease (after 3mm FG width).

#### D. Unbalanced Magnetic Force

Due to the asymmetric rotor structures, the unbalanced magnetic force (UMF) often exists in the CPMs and it is important to analyze the influence of FGs on the UMF. The open-circuit and the rated UMFs of all the modular CPMs versus FG width are shown in Fig. 12. In terms of the open-circuit UMFs, it can be seen that the C-core modular CPMs have much lower UMFs compared with those of the E-core modular CPMs, regardless of the FG width. The FG width generally has negative effect on the E-core machines which will increase the open-circuit UMF with increasing FG width. To explain this, the spectra of air-gap flux density only due to PMs in the 12-slot/14-pole E-core machines is shown in Fig. 13 (a). According to [20], the UMF is dependent on the working harmonic and its main sub-harmonics. It is found in Fig. 13 (a) that, although the 7<sup>th</sup> working harmonic reduces slightly with the FG width, the other harmonics such as 1<sup>st</sup>, 6<sup>th</sup>, 11<sup>th</sup>, 13<sup>th</sup>, etc. increase with the FG width. This contributes to the overall increase of the open-circuit UMFs in the E-core machines.

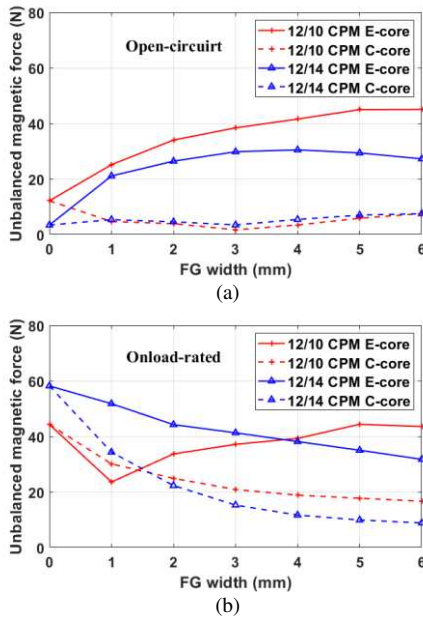


Fig. 12. Open-circuit and on-load UMFs vs FG width.

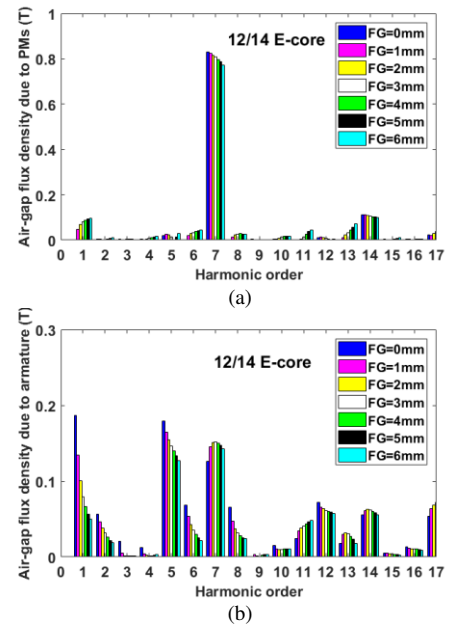


Fig. 13. Spectra of the air-gap flux densities (a) due to PMs only and (b) due to armature only of the E-core 12-slot/14-pole modular CPMs.

For the rated UMFs, except for some cases of the 12-slot/10-pole E-core machine, they can be significantly reduced by introducing FGs. Again, the spectra of air-gap flux density only due to armatures in the 12-slot/14-pole E-core machines are selected as an example. It can be seen that, although the 7<sup>th</sup> working harmonic varies slightly with the FG width, the 1<sup>st</sup>, 2<sup>nd</sup>, 5<sup>th</sup>, 6<sup>th</sup>, 8<sup>th</sup>, etc. harmonics all reduce with the FG width, leading to the overall reduced rated UMFs. To conclude, on one hand, the C-core structure can achieve much lower open-circuit UMF compared with the E-core structure, regardless of slot/pole number combinations. On the other hand, except for the 12-slot/10-pole E-core machine, the FGs can significantly reduce the on-load UMFs in all other machines and the 12-slot/14-pole C-core machines have the lowest UMFs.

#### E. Dynamic Characteristics

Apart from the above static electromagnetic characteristics, the dynamic performances are also key factors to evaluate the electrical machines. The dynamic characteristics such as torque-speed curves of all the investigated CPMs have been calculated, as shown in Fig. 14. For all the dynamic performance analyses in this section, it is assumed that the maximum inverter current (10.38A) and the maximum DC-bus voltage (40V) are the same for all the investigated modular CPMs.

It has found that the modular structure has almost no improvement for the flux-weakening capability of the 12-slot/10-pole E-core modular CPMs. For the 12-slot/10-pole C-core modular CPM, the flux weakening capability can even be worsened when the FG width equals to 2mm or 4mm. This is mainly due to the fact that the relatively higher phase flux linkages in comparison with the E-core modular CPMs can lead to higher  $\varphi_m/L_d$  which will result in a finite speed rather than infinite speed. However, due to the advantage of the flux-focusing effect of the modular structure, for the 12-slot/14-pole modular CPM machines, both the E-core and C-core structures can achieve better flux weakening capabilities by choosing

proper FG width while keeping the advantages of higher torque and power.

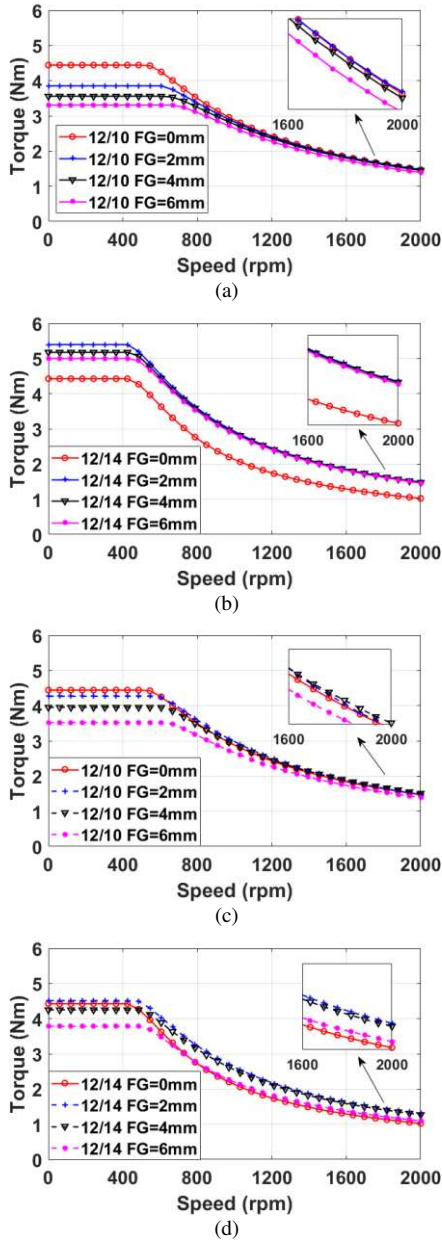


Fig. 14. Torque-speed curves of the 12-slot/10-pole and 12-slot/14-pole modular CPMs. (a) and (b) E-core CPM, (c) and (d) C-core CPM.

The above results have shown the influences of FG width on the dynamic performance of each machine, and it is important to have a comparison between different machines as well. Thus, the best candidate from each machine type (with optimal FG width) has been selected and shown in Fig. 15. Here the results such as power and power factor have been added to have a more comprehensive comparison. It is worth noting that both the 12-slot/10-pole and 14-pole non-modular machines (FG=0mm) have similar performances such as torque and power. Therefore, only the 12-slot/10-pole non-modular machines (FG=0mm) are shown in Fig. 15 (a) and (b). It is found that the 12-slot/14-pole E-core machine generally achieves the highest torque within the constant-torque region. Moreover, except the 12-slot/14-pole C-core machine, all other machines can have decent power factors over the full speed range.

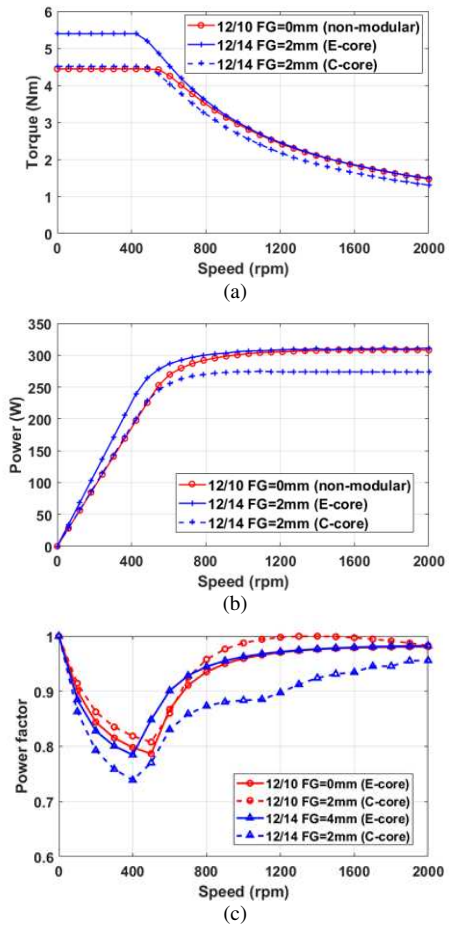


Fig. 15. Comparison of different machines in terms of dynamic performances (best candidate selected). (a) Torque-speed curves, (b) power-speed curves and (c) power factor-speed curves.

Last but not the least, the efficiency maps also play an important role in the dynamic performances. Therefore, the efficiency maps of the investigated E-core and C-core modular CPMs with different FG widths, e.g. FG=0mm, 2mm, 4mm and 6mm, have been calculated, and the results of E-core are shown in Fig. 16 and Fig. 17 as example. It is worth noting that the efficiency differences of the investigated modular CPMs are small which is mainly due to the relatively small size of the investigated machines leading to negligible PM eddy current losses. Nevertheless, the variation trend can be observed and some useful conclusions can be drawn.

For the 12-slot/10-pole E-core CPMs, the influence of FGs on the efficiency can be neglected. However, for all other machines, their efficiencies could be improved by selecting a proper FG width. For instance, the highest efficiencies of the 12-slot/14-pole E-core CPMs with 2mm, 4mm and 6mm FG width are 4% higher than that of the non-modular one, i.e. 0mm FG width. This is mainly due to the reduction in stator iron losses which has been elaborated in section IV.C. Due to the same reason, the 12-slot/10-pole C-core CPMs can achieve 2% improvement in the efficiencies while the efficiencies of the 12-slot/14-pole C-core CPMs can be 3% higher if an appropriate FG width is selected.

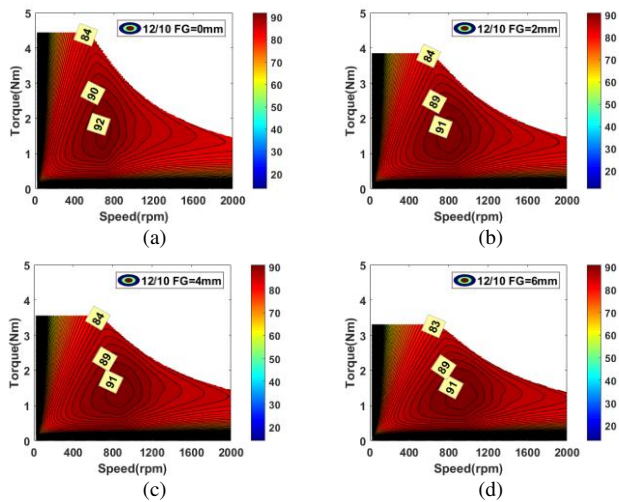


Fig. 16. Efficiency maps of the 12-slot/10-pole E-core CPMs with different FG widths. (a) FG=0mm, (b) FG=2mm, (c) FG=4mm, and (d) FG=6mm.

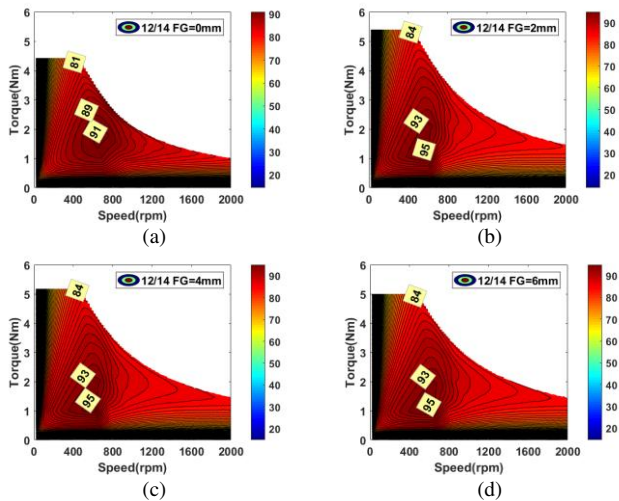


Fig. 17. Efficiency maps of the 12-slot/14-pole E-core CPMs with different FG widths. (a) FG=0mm, (b) FG=2mm, (c) FG=4mm, and (d) FG=6mm.

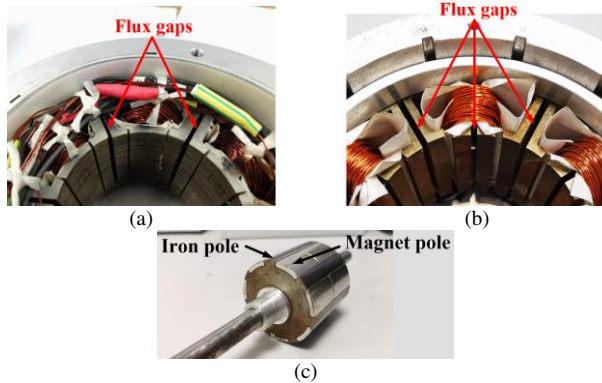


Fig. 18. Prototype modular machines with FG=2mm. (a) E-core stator, (b) C-core stator and (c) 14-pole CP rotor.

## V. EXPERIMENTAL VALIDATION

In order to verify the FEA predictions in the previous sections, both the 12-slot/14-pole E-core and C-core CPMs have been prototyped, as shown in Fig. 18, and their main dimensions are listed in Table 1. For both modular machines, the FG width is 2mm, which is a tradeoff between average

torque and copper losses (linked with slot area). In addition, they share a common 14-pole CP rotor, as shown in Fig. 18 (c).

### A. Phase back-EMFs

The phase back-EMFs of the prototype machines at 400rpm are measured and shown in Fig. 19. A generally good agreement between the predicted and measured results can be observed. The slight difference is mainly due to the fact that the end-effect of PMs have been neglected in the 2D FEA models [7].

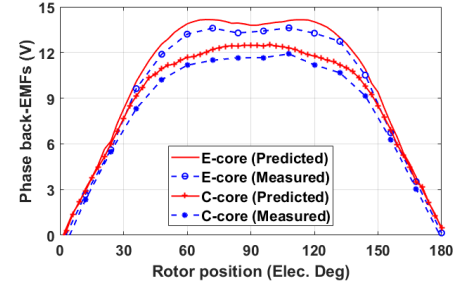


Fig. 19. Predicted and measured phase back-EMFs at 400rpm.

### B. Cogging Torques

The cogging torques are also measured using a well-established method introduced in [21]. It should be noted that for the 12-slot/14-pole C-core CPM, the discrepancy is mainly due to the small magnitude of the cogging torque, which makes the measurement process very difficult and hence a lower accuracy can be expected. Meanwhile, the manufacturing tolerance may also contribute to the slight difference between the predicted and measured results.

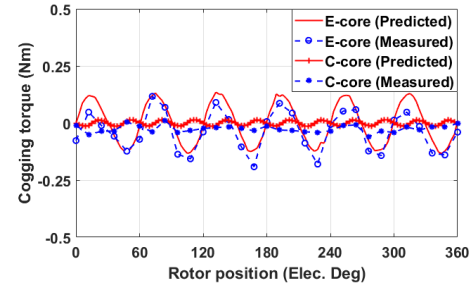


Fig. 20. Predicted and measured cogging torques.

### C. Static Torques

The on-load static torque has also been measured using similar method as for measuring the cogging torque. Here the machines are supplied with 3-phase currents  $I_A = I$ ,  $I_B = -I/2$  and  $I_C = -I/2$ , where  $I$  is a dc current, which can be changed to simulate different load conditions.  $I$  also represents the current amplitude of an equivalent 3-phase sinewave current supply. To avoid possible overheating of the prototype machines, 3A is selected as the dc current to obtain the waveform of static torque versus rotor position, as shown in Fig. 21. It is worth noting that the different rotor positions are equivalent to the changing current phase angle in a 3-phase sinewave current supply. Moreover, at a fixed rotor position where the static torque is maximum, the static torques under different phase peak currents have also been measured and compared with the predicted results, as shown in Fig. 22.

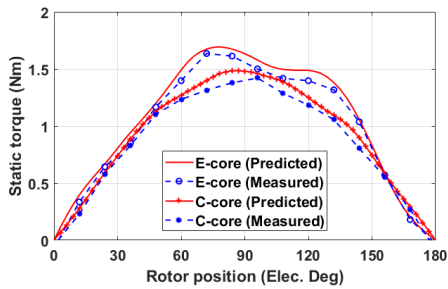


Fig. 21. Predicted and measured static torques vs rotor position with  $I_A = 3A$ ,  $I_B = I_C = -1.5A$ .

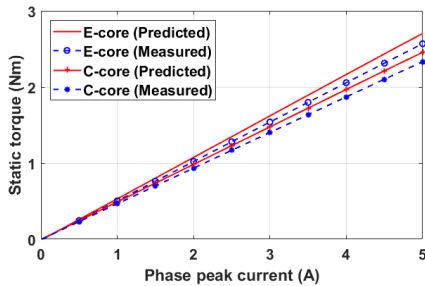


Fig. 22. Predicted and measured static torques vs phase peak current.

#### D. Dynamic Tests

The torque-speed curves of the prototypes have also been measured and compared with the predicted ones, as shown in Fig. 23. The dc link voltage is set to be 18 V and the peak phase current is 6 A, which is limited by the inverter capacity. The slight difference between the predicted and measured results is largely due to the end-winding effect and also phase voltage distortion that have not been accounted for in the simulations.

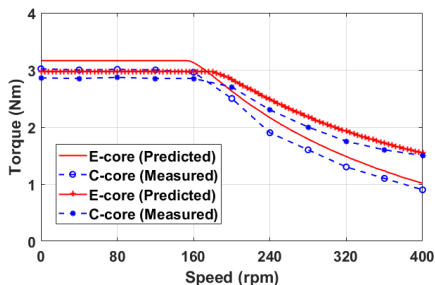


Fig. 23. Predicted and measured torque-speed curves.

## VI. CONCLUSION

This paper investigates some novel modular consequent pole PM machines (CPMs) with both E-core and C-core stators. Two typical slot/pole number combinations including 12-slot/10-pole ( $N_s > 2p$ ) and 12-slot/14-pole ( $N_s < 2p$ ) have been taken into consideration. Using finite element simulations, the influences of flux gap (FG) width on static (back-EMF, cogging torque, UMF, etc.) and dynamic performances (torque/power speed curves, efficiency maps) of these modular CPMs have been investigated. The simulated static and dynamic performances have been validated by a series of experimental tests.

In order to select the best modular CPMs for different applications with different requirements, the following design guidelines and recommendations can be adopted:

- Best candidate for maximizing the average torque: 12-slot/14-pole with E-core, the average torque increases by 17.3% from 4.4Nm (FG=0mm) to 5.2Nm (FG=3mm).

- Best candidate for minimizing torque ripple: 12-slot/10-pole with C-core, the torque ripple reduces by 68.7% from 9.4Nm (FG=0mm) to 2.9Nm (FG=3mm).
- Best candidate for minimizing on-load UMF: 12-slot/14-pole with C-core, the UMF reduces by 84.8% from 58.2N (FG=0mm) to 8.8N (FG=6mm).
- Best candidate for achieving the highest efficiency: 12-slot/14-pole with E-core, the efficiency increases by 4% from 91% (FG=0mm) to 95% (FG=2mm).
- Best candidates for achieving the optimal dynamic performances are recommended in Table 3.

Table 3 Best candidates for dynamic performances

Flux-weakening capability	Power factor
12-slot/14-pole E-core (FG=2mm)	12-slot/10-pole E-core (FG=2mm)

## REFERENCES

- [1] K. T. Chau, C. C. Chan, and C. Liu, "Overview of permanent-magnet brushless drives for electric and hybrid electric vehicles," *IEEE Trans. Ind. Electron.*, vol. 55, pp. 2246-2257, Jun. 2008.
- [2] S. U. Chung, J. W. Kim, Y. D. Chun, B. C. Woo, and D. K. Hong, "Fractional slot concentrated winding PMSM with consequent pole rotor for a low-speed direct drive: reduction of rare earth permanent magnet," *IEEE Trans. Energy Convers.*, vol. 30, pp. 103-109, Sep. 2015.
- [3] Y. Gao, R. Qu, D. Li, J. Li, and G. Zhou, "Consequent-pole flux-reversal permanent-magnet machine for electric vehicle propulsion," *IEEE Trans. Appl. Supercond.*, vol. 26, pp. 1-5, Jun. 2016.
- [4] Z. Z. Wu and Z. Q. Zhu, "Partitioned stator flux reversal machine with consequent-pole PM stator," *IEEE Trans. Energy Convers.*, vol. 30, pp. 1472-1482, Jan. 2015.
- [5] Q. Wang, S. Niu, and X. Luo, "A novel hybrid dual-PM machine excited by AC with DC bias for electric vehicle propulsion," *IEEE Trans. Ind. Electron.*, vol. 64, pp. 6908-6919, 2017.
- [6] F. Li, K. Wang, J. Li, and H. J. Zhang, "Suppression of even-order harmonics and torque ripple in outer rotor consequent-pole PM machine by multilayer winding," *IEEE Trans. Magn.*, pp. 1-5, Jun. 2018.
- [7] J. Li, K. Wang, F. Li, S. Zhu, and C. Liu, "Elimination of even-order harmonics and unipolar leakage flux in consequent-pole PM machines by employing N-S-iron-S-N-iron rotor," *IEEE Trans. Ind. Electron.*, pp. 1-1, May 2018.
- [8] J. Li, K. Wang, and C. Liu, "Comparative study of consequent-pole and hybrid-pole permanent magnet machines," *IEEE Trans. Energy Convers.*, vol. 34, pp. 701-711, 2019.
- [9] J. Li, K. Wang, and H. Zhang, "Flux-focusing permanent magnet machines with modular consequent-pole rotor," *IEEE Trans. Ind. Electron.*, vol. 67, pp. 3374-3385, 2020.
- [10] J. Li, K. Wang, and C. Liu, "Torque improvement and cost reduction of permanent magnet machines with a dovetailed consequent-pole rotor," *IEEE Trans. Energy Convers.*, vol. 33, pp. 1628-1640, 2018.
- [11] E. Spooner, A. C. Williamson, and G. Catto, "Modular design of permanent-magnet generators for wind turbines," *IEE Proc.-Electr. Power Appl.*, vol. 143, pp. 388-395, Sep. 1996.
- [12] S. Jianxin, W. Canfei, M. Dongmin, J. Mengjia, S. Dan, and W. Yunchong, "Analysis and optimization of a modular stator core with segmental teeth and solid back iron for pm electric machines," presented at the IEEE International Electric Machines & Drives Conference (IEMDC), 2011.
- [13] G. Dajaku, X. Wei, and D. Gerling, "Reduction of low space harmonics for the fractional slot concentrated windings using a novel stator design," *IEEE Trans. Magn.*, vol. 50, pp. 1-12, Dec. 2014.
- [14] G. J. Li, Z. Q. Zhu, W. Q. Chu, M. P. Foster, and D. A. Stone, "Influence of flux gaps on electromagnetic performance of novel modular PM machines," *IEEE Trans. Energy Convers.*, vol. 29, pp. 716-726, April. 2014.
- [15] G. J. Li, Z. Q. Zhu, M. Foster, and D. Stone, "Comparative studies of modular and unequal tooth PM machines either with or without tooth tips," *IEEE Trans. Magn.*, vol. 50, pp. 1-10, March. 2014.
- [16] G. J. Li, Z. Q. Zhu, M. P. Foster, D. A. Stone, and H. L. Zhan, "Modular permanent-magnet machines with alternate teeth having tooth tips," *IEEE Trans. Ind. Electron.*, vol. 62, pp. 6120-6130, April. 2015.
- [17] B. Ren, G. Li, Z. Zhu, M. Foster, and D. Stone, "Performance comparison between consequent-pole and inset modular permanent magnet

- machines," *The Journal of Engineering*, vol. 2019, pp. 3951-3955, Jun. 2019.
- [18] S. Cai, Z. Q. Zhu, C. Wang, J. C. Mipo, and S. Personnaz, "A novel fractional slot non-overlapping winding hybrid excited machine with consequent-pole PM rotor," *IEEE Trans. Energy Convers.*, pp. 1-1, 2020.
- [19] Z. Q. Zhu and D. Howe, "Influence of design parameters on cogging torque in permanent magnet machines," *IEEE Trans. Energy Convers.*, vol. 15, pp. 407-412, Dec. 2000.
- [20] Y. Wang, Z. Q. Zhu, J. Feng, S. Guo, Y. F. Li, and Y. Wang, "Investigation of unbalanced magnetic force in fractional-slot PM machines having an odd number of stator slots," *IEEE Trans. Energy Convers.*, pp. 1-1, May 2020.
- [21] Z. Q. Zhu, "A simple method for measuring cogging torque in permanent magnet machines," in *2009 IEEE Power & Energy Society General Meeting*, 2009, pp. 1-4.